Actively Controlled Trajectory Folding for Microwave Ramsey Interrogation Using a Moving Optical Lattice

Chunwei Wang(王春唯)[1], Yi Liang(梁毅)[1], Jielong Du(杜杰龙)[2], Yiheng Li(李亦恒)[1], Qing Wang(王青)[1], and Xiaoji Zhou(周小计)[1,2,*]

[1]State Key Laboratory of Photonics and Communications, School of Electronics, Peking University, Beijing 100871, China

[2]Institute of Carbon-based Thin Film Electronics, Peking University, Taiyuan 030012, China

Abstract

Microwave Ramsey interrogation with ultracold atoms is an important tool for coherent manipulation and precision measurement. Its frequency resolution improves with increasing free evolution time. However, in a compact geometry the usable Ramsey time is limited by the available trajectory length of the atomic motion. Here we combine Bloch oscillations in a moving optical lattice with microwave Ramsey interrogation of ultracold ^{87}Rb atoms and demonstrate a single-fold trajectory folding scheme. In this sequence, the moving optical lattice is applied between two microwave $\pi/2$ pulses and provides upward momentum compensation to the falling ultracold atoms, directing them back to the microwave interaction region for the second Ramsey pulse. Ramsey spectra recorded without and with lattice-assisted trajectory control show that the moving lattice can be incorporated into the Ramsey sequence while maintaining a reproducible Ramsey interference signal. With single-fold trajectory folding, the free evolution time is extended to 151 ms, and a Ramsey linewidth of 3.12 ± 0.07 Hz is obtained, comparable to the linewidth scale set by the inverse of the Ramsey time. These results demonstrate actively controlled trajectory folding for microwave Ramsey interrogation of ultracold atoms and provide a possible route for long coherent evolution in a limited spatial volume.

Keywords: Moving Optical Lattice, Microwave Ramsey Interrogation, Bloch Oscillations, Trajectory Folding
PACS: 37.10.Jk, 37.25.+k, 06.30.Ft, 03.75.Dg

1. Introduction

Microwave Ramsey interrogation is a key technique for coherent manipulation and precision measurement with ultracold atoms [1]. In a Ramsey sequence, the frequency resolution is primarily determined by the free evolution time T between two microwave $\pi/2$ pulses, with the central fringe linewidth approximately following $\Delta\nu \simeq 1/(2T)$ [1–5]. Extending T is a direct way to narrow the Ramsey fringes and improve frequency discrimination. In compact ultracold-atom systems, however, the attainable interrogation time is limited by the available space for atomic motion [6–12]. This makes trajectory management an important issue for long-time Ramsey interrogation in a limited spatial volume.

A natural way to increase the interrogation time in a limited volume is to fold the atomic trajectory. Conventional fountain geometries can be regarded as a passive form of trajectory folding, in which atoms are launched upward and return under gravity after a single ballistic turning point [3, 4]. This approach is well established, but the trajectory is fixed by the launch condition and gravity; for a given apparatus size, the Ramsey time is therefore set by the ballistic geometry, and the single turning point cannot naturally provide repeated trajectory folds. An alternative route is to actively control the atomic motion during the Ramsey interval. Bloch oscillations in a moving optical lattice provide coherent momentum transfer and have been widely used in atom interferometry, large-momentum-transfer beam splitting, and atomic transport [13–24]. Related fieldable atom-interferometric schemes and Raman-based matter-wave interferometers provide a broader context for trajectory and phase control with ultracold atoms [25–29]. Our previous studies have established key techniques related to spatially correlated lattice interferometry, atomic Bloch oscillations, accelerated and moving optical lattices, optical-lattice loading, optical-lattice Ramsey interferometry, and Bloch-state control [30–37]. These works show that optical lattices can provide precise control of the external motion and motional quantum states of ultracold atoms. However, to our knowledge, Bloch-oscillation-based trajectory folding using a moving optical lattice has not yet been integrated with microwave Ramsey interrogation, where internal-state coherence

*Corresponding author. E-mail: xjzhou@pku.edu.cn

must be preserved while the lattice controls the external atomic motion within the same experimental sequence.

Here, using ultracold ^{87}Rb atoms, we combine Bloch-oscillation-based trajectory control with microwave Ramsey interrogation and experimentally demonstrate a single-fold trajectory folding scheme. A moving optical lattice is inserted between two microwave Ramsey pulses to provide upward momentum compensation and direct the falling ultracold atoms back to the microwave interaction region. The experiment is designed to establish three points: first, the moving optical lattice can redirect the atomic trajectory within a centimeter-scale region; second, the lattice operation can be incorporated into the microwave Ramsey sequence while maintaining a reproducible Ramsey fringe; and third, the same single-fold trajectory control sequence can extend the Ramsey free evolution time beyond the practical free-fall boundary of the present apparatus. The measured Ramsey linewidth reaches 3.12 ± 0.07 Hz at $T = 151$ ms. The emphasis of this work is not to outperform a conventional fountain at the same Ramsey time, but to show that a purely ballistic Ramsey trajectory can be replaced by an actively controlled one that can be further extended toward multiple-fold operation.

2. Principle and experimental method

2.1. Ramsey linewidth and the compact-space limitation

For a microwave Ramsey sequence, two separate $\pi/2$ pulses convert the phase accumulated during the free evolution time T into a population difference. The linewidth of the central Ramsey fringe approximately follows

$$\Delta\nu \simeq \frac{1}{2T}. \tag{1}$$

Thus, increasing T is the most direct way to narrow the Ramsey fringe. Equation (1) characterizes the linewidth scale, but extending the usable Ramsey time also requires that the fringe modulation and phase remain sufficiently well defined. We therefore quantify the linewidth, fringe modulation depth, and measurement scatter in the experimental results below.

In a compact apparatus, the Ramsey time cannot be extended indefinitely in passive ballistic motion. A fountain trajectory provides a single gravity-induced turning point and its usable interrogation time is set by the available spatial scale. The present approach instead redirects the atoms during the Ramsey interval, providing an actively controlled trajectory fold within the same confined region.

2.2. Moving optical lattice trajectory folding

This active folding operation is implemented by applying a moving optical lattice between two microwave $\pi/2$ pulses. After the first Ramsey pulse, the atoms begin to fall under gravity. The optical lattice then transfers upward momentum through Bloch oscillations, redirects the atomic motion, and brings the atoms back toward the microwave interaction region for the second Ramsey pulse. The basic idea of active trajectory folding is illustrated in Fig. 1. The horizontal axis represents time, and the vertical axis represents the atomic position along the direction of gravity. In the upper panel, the black trajectory illustrates a representative passive fountain geometry. The two yellow vertical regions denote the two microwave $\pi/2$ pulses, and the purple region denotes the probe-light detection window. In this passive case, a Ramsey time of about $T = 0.5$ s requires a vertical trajectory scale of about 30 cm, as indicated on the right side of the figure.

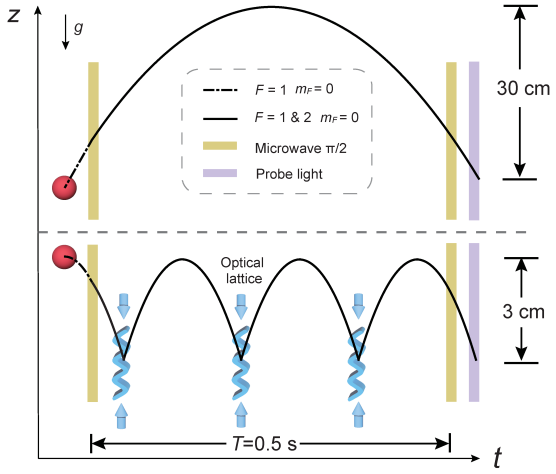


Fig. 1. Concept of actively controlled trajectory folding for microwave Ramsey interrogation. The horizontal axis denotes time and the vertical axis denotes the atomic position along gravity. Yellow vertical regions represent the microwave $\pi/2$ pulses, purple regions represent probe-light detection windows, black curves represent atomic trajectories, and blue wavy structures represent moving optical lattice pulses. The upper panel shows a representative passive fountain trajectory, where a Ramsey time of $T \approx 0.5$ s corresponds to a vertical scale of about 30 cm. The lower panel shows the moving optical lattice trajectory folding scheme, in which Bloch oscillations redirect the falling ultracold atoms and guide them back to the microwave interaction region within a vertical scale of about 3 cm. The present experiment demonstrates one trajectory folding cycle, while the repeated lattice pulses schematically indicate the possible extension to multiple-fold.

The lower panel shows the active trajectory folding scheme. After the first microwave $\pi/2$ pulse, the ultracold atoms fall under gravity. The blue wavy structures denote the moving optical lattice. During the Ramsey interval, the moving lattice transfers upward momentum to the atoms by Bloch oscillations. As a result, the atomic trajectory is redirected and folded within a much smaller vertical scale of only about 3 cm, so that the atoms return to the microwave interaction region for the second $\pi/2$ pulse. The present experiment realizes one folding cycle, while the repeated lattice pulses in the schematic indicate a possible extension toward multiple-fold operation.

The moving optical lattice is generated by

two counter-propagating Bloch beams with a time-dependent frequency difference. In the accelerated lattice frame, atoms adiabatically follow the lattice potential and acquire momentum by Bloch oscillations. For N Bloch oscillations, the total momentum and velocity changes are

$$\Delta p = 2N\hbar k, \tag{2}$$

$$\Delta v = 2Nv_{\mathrm{r}}, \qquad v_{\mathrm{r}} = \frac{\hbar k}{m}, \tag{3}$$

where $k = 2\pi/\lambda$ is the wave number of the Bloch light, m is the atomic mass, and v_{r} is the single-photon recoil velocity. By choosing the sweep range, sweep duration, and lattice depth, the upward velocity compensation can be matched to the free-fall trajectory between the two Ramsey pulses.

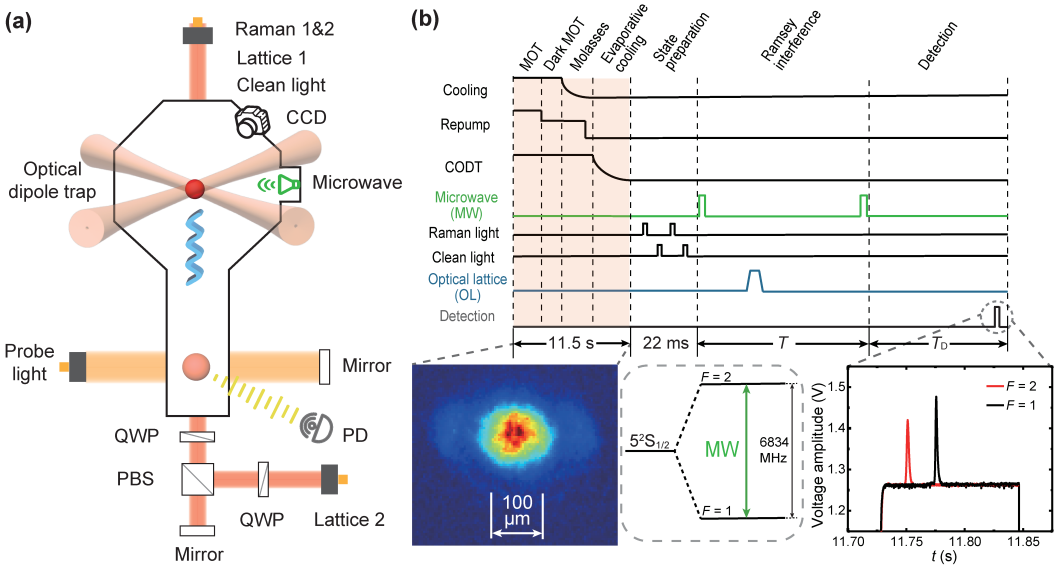


Fig. 2. Experimental realization of microwave Ramsey interrogation with optical-lattice trajectory control. (a) Schematic of the apparatus. Raman beams and clean light are used for state preparation, the microwave horn provides the Ramsey $\pi/2$ pulses, Lattice 1 and Lattice 2 form the vertical moving optical lattice for Bloch-oscillation momentum transfer, and probe light together with the photodetector is used for state-selective detection. (b) Experimental timing sequence including magneto-optical trap (MOT) loading, molasses cooling, evaporative cooling, state preparation, microwave Ramsey interrogation, optical-lattice operation, and final detection. The lower insets show, from left to right, a representative absorption image of the ultracold ^{87}Rb sample, the microwave transition between the $F = 1$ and $F = 2$ ground-state hyperfine levels, and representative state-selective detection signals for the two hyperfine states.

2.3. Experimental setup and sequence

The experiment was implemented by adapting an existing Bloch-oscillation-based atom gravimeter platform for microwave Ramsey interrogation. The original platform provides efficient preparation of ultracold ^{87}Rb atoms and well-controlled optical lattice momentum transfer, while the added microwave system provides the two Ramsey $\pi/2$ pulses used in the present trajectory folding sequence. Since the present experiment focuses on combining microwave Ramsey coherent evolution with optical lattice trajectory control rather than realizing an optimized clock package, the microwave field is delivered by direct radiation from a microwave horn instead of a cavity. The experimental apparatus is summarized in Fig. 2. The ultracold ^{87}Rb sample is first prepared in the optical dipole trap. Raman beams and clean light are used for state preparation and the removal of unwanted atomic populations. The microwave horn provides the two Ramsey $\pi/2$ pulses. Two counter-propagating lattice beams, labeled Lattice 1 and Lattice 2, form the vertical moving optical lattice for momentum transfer through Bloch oscillations. After the Ramsey sequence, probe light and a photodetector are used for state detection.

The atomic sample is prepared by standard laser-cooling, evaporative-cooling, and optical-trapping techniques [38–42]. Typical samples contain about 2×10^5 atoms at a temperature of approximately 51 nK. The temperature is extracted from the absorption images by fitting the expanded atomic density distribution. State preparation is performed using optical pumping, Raman light, and clean light, preparing the atoms for microwave interrogation on the magnetically insensitive $|5^2S_{1/2}, F = 1, m_F = 0\rangle \leftrightarrow |5^2S_{1/2}, F = 2, m_F = 0\rangle$ ground-state hyperfine transition near 6.834 GHz, as illustrated in Fig. 2(b). State-selective detection is performed using fluorescence detection. The probe light is resonant with the $5^2S_{1/2}, F = 2 \rightarrow 5^2P_{3/2}, F' = 3$ cycling transition, while the repump light addresses the $5^2S_{1/2}, F = 1 \rightarrow 5^2P_{3/2}, F' = 2$ transition. The transition probability used throughout this work is defined

as

$$P = \frac{N_2}{N_1 + N_2}, \tag{4}$$

where N_1 and N_2 denote the detected atom numbers in the $F = 1$ and $F = 2$ ground-state hyperfine levels, respectively.

The timing sequence in Fig. 2(b) shows how the moving optical lattice is incorporated into the Ramsey interrogation. After MOT loading, molasses cooling, evaporative cooling, and state preparation, the first microwave $\pi/2$ pulse creates a coherent superposition of the two clock states. In the lattice-assisted sequence, a moving-optical-lattice pulse is inserted during the Ramsey free-evolution time to compensate the downward velocity acquired under gravity. As described by Eqs. (2) and (3), the moving lattice provides Bloch-oscillation-based momentum transfer, and the resulting velocity change provides the upward momentum compensation required to redirect the falling atoms toward the microwave-interaction region. The second microwave $\pi/2$ pulse then converts the accumulated phase into a population difference, which is measured after a detection delay T_D. In the free-fall reference sequence, the same microwave and detection procedures are used, but the optical-lattice pulse is omitted.

The two counter-propagating Bloch beams operate at 780 nm. The lattice depth and frequency-sweep waveform are experimentally optimized to provide efficient Bloch momentum transfer while limiting lattice-induced decoherence. In the optimized narrow-linewidth measurements, the lattice depth is reduced relative to the earlier trajectory-manipulation condition in order to suppress differential light shifts and additional phase accumulation induced by the lattice.

3. Results

The measurements are presented in the order in which the trajectory folding operation is established experimentally. We first characterize the free-fall Ramsey response of the modified apparatus and determine its practical linewidth boundary. We then apply the moving optical lattice at $T = 50$ ms, where the free-fall Ramsey reference remains reliably measurable, and compare the Ramsey spectra without and with lattice-assisted trajectory control. Finally, we increase the free evolution time using the single-fold trajectory control sequence and analyze the resulting linewidth narrowing.

3.1. Free-fall reference and practical linewidth boundary

We first characterize the usable Ramsey-time range without optical-lattice trajectory control. At relatively short free-evolution times, the atomic cloud remains within the effective microwave-interaction region, so that the two Ramsey pulses can be applied under comparable conditions. At $T = 50$ ms, a clear Ramsey fringe is obtained with a fitted linewidth of 10.16 ± 0.27 Hz, providing a reliable free-fall reference for comparison with the lattice-assisted sequence.

When the free-evolution time is increased toward the nominal 5-Hz linewidth regime, however, no reliable fitted linewidth can be extracted from the free-fall configuration under the same experimental and fitting procedure. We therefore take the vicinity of this regime as the practical free-fall boundary of the present compact apparatus. This boundary provides the experimental motivation for active trajectory folding: the moving lattice should redirect the atoms so that the second Ramsey pulse can still be applied effectively at longer T.

3.2. Lattice-assisted 10 Hz Ramsey fringes

We next compare Ramsey fringes at $T = 50$ ms, corresponding to a nominal 10-Hz linewidth, with and without the moving optical lattice. At this Ramsey time, the free-fall reference remains reliably measurable, allowing the influence of the lattice-assisted trajectory-control operation to be evaluated under otherwise similar state-preparation and detection conditions. The point-to-fit scatter is examined here because extending the usable Ramsey interrogation requires not only a measurable fringe modulation but also a sufficiently well-defined interference pattern for reliable extraction of the spectral parameters.

Fig. 3 summarizes the comparison. Figs. 3(a) and 3(b) show the transition probability as a function of microwave detuning for the free-fall and lattice-assisted sequences, respectively. Each point represents one individual experimental measurement at the corresponding detuning, and the solid curves are Ramsey-fringe fits. The fitted linewidths are 10.16 ± 0.27 Hz without the lattice and 10.07 ± 0.08 Hz with the lattice.

To quantify the fringe modulation, we define the peak-to-peak modulation depth as

$$\Delta P = 2A, \tag{5}$$

where A is the sinusoidal amplitude obtained from the Ramsey-fringe fit. The scatter of the individual measurements about the fitted fringe is quantified by the root-mean-square (RMS) residual

$$\sigma_{\mathrm{RMS}} = \sqrt{\frac{1}{N}\sum_{i=1}^{N}\left[P_i - P_{\mathrm{fit}}(\delta_i)\right]^2}, \tag{6}$$

where P_i is the measured transition probability at detuning δ_i, $P_{\mathrm{fit}}(\delta_i)$ is the corresponding fitted value, and N is the number of data points included in the fit.

For the free-fall measurement, the fitted modulation depth is $\Delta P = 0.586 \pm 0.054$, and the RMS residual is 0.112, with $R^2 = 0.77$. With the moving lattice applied at the same free-evolution time, the modulation depth decreases to $\Delta P = 0.375 \pm 0.011$, whereas the RMS residual decreases to 0.0233 and the coefficient of determination increases to $R^2 = 0.97$. The two quantities describe different aspects of the measured fringe: the smaller modulation depth indicates reduced Ramsey-fringe modulation associated with the lattice-assisted

operation, whereas the smaller RMS residual indicates reduced point-to-fit scatter and better agreement with the fitted Ramsey-fringe model.

The larger point-to-fit scatter in the free-fall data may arise, at least in part, from trajectory-dependent sampling of the spatially nonuniform microwave field. In the free-fall sequence, the atoms continue to move downward before the second microwave $\pi/2$ pulse. Small experimental variations in the atomic position and velocity distribution can therefore translate into variations in the position at which the second microwave interaction occurs and, because the microwave field is delivered by a horn, in the microwave amplitude and phase sampled by the atoms. In the lattice-assisted sequence, trajectory redirection guides the atoms back to the microwave-interaction region and can make the conditions of the second microwave interaction more reproducible from one experimental realization to another. This provides a plausible contribution to the smaller RMS residual observed with the lattice. Other technical fluctuations, including slow changes in the magnetic field, microwave source amplitude or phase, and state-preparation or detection conditions, may also contribute to the observed difference. However, we emphasize that the free-fall and lattice-assisted spectra were acquired in independent scans rather than as an interleaved noise comparison. The present data therefore do not establish a unique origin of the difference in scatter or a quantitative noise budget.

The trajectory difference is illustrated in Figs. 3(a1) and 3(b1). In the free-fall case, the atoms continue to move downward between the two microwave pulses. In the lattice-assisted case, the blue vertical region denotes the optical-lattice operation, which redirects the atomic motion before the second microwave pulse. Fig. 3(c) shows repeated lattice-assisted measurements over eight experimental runs. The fitted linewidth and initial phase exhibit only small run-to-run variations, demonstrating the reproducibility of the lattice-assisted Ramsey signal at the 10-Hz level.

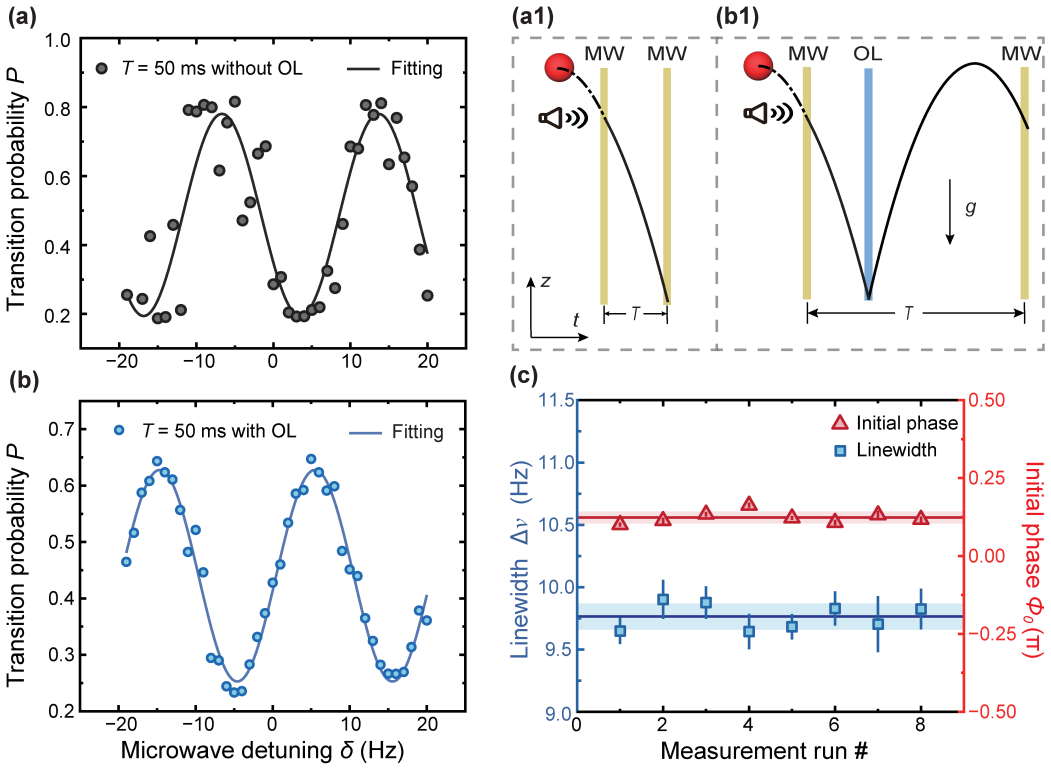


Fig. 3. Comparison of 10 Hz Ramsey fringes without and with lattice-assisted trajectory folding. (a) Ramsey fringe obtained without the optical lattice for a free evolution time of $T = 50$ ms. (b) Ramsey fringe obtained with the moving optical lattice inserted between the two microwave pulses at the same free evolution time. In (a) and (b), each dot represents one individual experimental measurement at the corresponding detuning, and the solid curves are Ramsey-fringe fits. (a1) Schematic trajectory without the optical lattice, where the atoms continue to fall between the two microwave pulses. (b1) Schematic trajectory with the optical lattice, where the blue region indicates lattice-assisted momentum compensation and trajectory folding. (c) Repeated lattice-assisted measurements over eight experimental runs. Blue squares represent the fitted linewidth $\Delta\nu$, red triangles represent the fitted initial phase ϕ_0, and horizontal lines indicate the corresponding mean values.

3.3. Extension of Ramsey time by single-fold trajectory control

After obtaining reproducible lattice-assisted Ramsey fringes at the 10-Hz level, we increase the free-evolution time toward and beyond the practical free-fall boundary. At $T = 100$ ms, corresponding to a nominal 5-Hz linewidth, the free-fall configuration does not yield a reliable fitted linewidth under the same fitting procedure.

With the moving optical lattice applied, the atoms are redirected toward the microwave-interaction region and a clear Ramsey fringe is obtained. The corresponding spectrum is shown in the left inset of Fig. 4, with a fitted linewidth of $\Delta\nu = 4.58 \pm 0.09$ Hz and a peak-to-peak modulation depth of $\Delta P = 0.320 \pm 0.022$.

The trajectory-control sequence is then further optimized for a longer Ramsey time. The lattice depth is reduced relative to the earlier trajectory-manipulation condition to mitigate differential AC Stark shifts and lattice-induced phase accumulation. The lattice loading and frequency-sweep parameters are experimentally adjusted to improve Bloch momentum transfer and trajectory control, and the state-preparation sequence is refined to reduce residual populations in unwanted magnetic sublevels. With these optimized trajectory-control settings, the free-evolution time is extended to $T = 151$ ms.

The right inset of Fig. 4 shows the corresponding Ramsey spectrum at $T = 151$ ms. A fitted linewidth of $\Delta\nu = 3.12 \pm 0.07$ Hz is obtained, comparable to the inverse-time reference scale $1/(2T) = 3.31$ Hz. The corresponding peak-to-peak modulation depth is $\Delta P = 0.199 \pm 0.017$. Together with the value $\Delta P = 0.375 \pm 0.011$ at $T = 50$ ms, these results show that the Ramsey linewidth continues to narrow as the controlled interrogation time is extended, while the fringe modulation depth progressively decreases.

3.4. Linewidth scaling with free evolution time

Fig. 4 summarizes the linewidth narrowing obtained in the experiment. The horizontal axis is the Ramsey free evolution time T, and the vertical axis is the fitted Ramsey linewidth $\Delta\nu$. The black solid curve represents the inverse-time reference scaling $\Delta\nu = 1/(2T)$ and is used to guide the expected linewidth narrowing with increasing Ramsey time. The open black squares denote free-fall Ramsey measurements without optical lattice trajectory control, while the blue squares denote measurements with the moving optical lattice. The blue circles in the two insets are the measured Ramsey spectra at longer T, and the blue solid curves are the corresponding fits. The gray dashed lines serve as guides connecting the main linewidth points to the spectra shown in the insets.

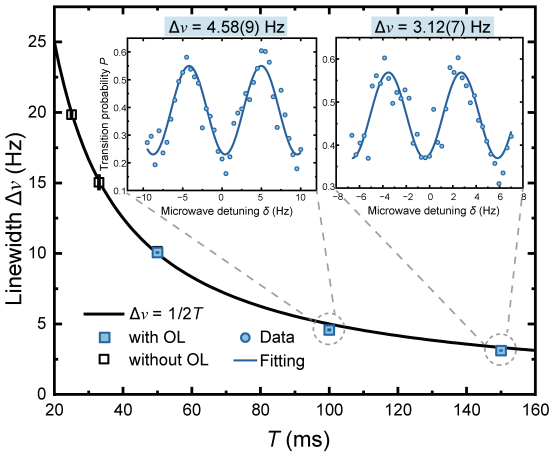


Fig. 4. Ramsey linewidth narrowing enabled by moving optical lattice trajectory control. The black solid curve represents the inverse-time reference scaling $\Delta\nu = 1/(2T)$. Open black squares denote measurements without optical lattice control, and blue squares indicate lattice-assisted measurements. The insets show representative Ramsey spectra at longer free evolution times; blue circles are experimental data and blue solid curves are fits. The final lattice-assisted measurement at $T = 151$ ms yields $\Delta\nu = 3.12 \pm 0.07$ Hz.

Without lattice control, stable fitted fringes are obtained only in the relatively short-T range. As T approaches the nominal 5 Hz linewidth region, the free-fall configuration reaches the practical boundary of the present compact apparatus. With trajectory control provided by the moving lattice, Ramsey fringes are obtained at longer free evolution times. The lattice-assisted data follow the expected inverse-time narrowing trend with increasing T, indicating that the linewidth narrowing mainly results from the extended Ramsey evolution time. The final data point at $T = 151$ ms corresponds to the single-fold trajectory control sequence and gives a linewidth of 3.12 ± 0.07 Hz.

4. Discussion

4.1. Role of actively controlled trajectory folding

The results above demonstrate that momentum transfer based on Bloch oscillations can be integrated with microwave Ramsey coherent evolution to realize actively controlled trajectory folding. The measured Ramsey linewidth of 3.12 ± 0.07 Hz shows that the trajectory-control operation extends the effective free-evolution time of the compact apparatus while retaining a clearly resolvable Ramsey interference signal.

It is important to note that the present experiment demonstrates only a single trajectory folding cycle. A conventional fountain trajectory also contains a single ballistic turning point, and therefore the achieved interrogation time and linewidth are comparable to those obtainable in a fountain geometry with a similar free evolution time. The significance of the present method does not lie in surpassing fountain performance at the single-fold stage, but in replacing a purely ballistic trajectory with an actively controlled one.

This distinction is essential for future extensions. In a ballistic fountain, the trajectory is determined by the initial launch velocity and gravity. In the present scheme, the atomic motion is modified during the Ramsey interval by momentum transfer from the optical lattice. This active controllability provides the physical basis for future multiple-fold trajectory cycles within a confined spatial region, provided that the associated decoherence mechanisms can be sufficiently suppressed.

4.2. Present limiting factors

The quantitative fringe analysis reveals a clear trade-off associated with lattice-assisted trajectory control. At $T = 50$ ms, introducing the moving lattice reduces the peak-to-peak modulation depth from 0.586 ± 0.054 to 0.375 ± 0.011, while the RMS residual decreases from 0.112 to 0.0233. As the lattice-assisted Ramsey time is extended, the modulation depth further decreases to 0.320 ± 0.022 at $T = 100$ ms and 0.199 ± 0.017 at $T = 151$ ms. These observations show that trajectory folding removes the immediate spatial limitation of the free-fall configuration, whereas preservation of the Ramsey-fringe modulation becomes increasingly important for longer controlled trajectories. A quantitative separation of the underlying decoherence mechanisms is not available in the present experiment, but several contributions are relevant.

First, the moving optical lattice can introduce both lattice-induced dephasing and a shift of the Ramsey fringe. The differential AC Stark shift between the two clock states produces an additional phase during the lattice interaction,

$$\phi_{\mathrm{lat}} = 2\pi \int_{t_i}^{t_f} \Delta\nu_{\mathrm{AC}}(t)\, dt,$$

where $\Delta\nu_{\mathrm{AC}}(t)$ is the instantaneous differential AC Stark shift. In an ideal Ramsey description, the fringe can be written as

$$P(\delta) = P_0 + A\cos[2\pi\delta T + \phi_{\mathrm{ref}} + \phi_{\mathrm{lat}}]\,,$$

where δ is the microwave detuning and ϕ_{ref} denotes the Ramsey phase accumulated in the absence of the lattice-induced contribution. A spatially and temporally uniform lattice-induced phase therefore appears as a horizontal displacement of the Ramsey fringe, corresponding to

$$\Delta\delta_{\mathrm{lat}} = -\frac{\phi_{\mathrm{lat}}}{2\pi T},$$

up to the sign convention used for the Ramsey phase. Thus, a common lattice-induced phase can shift the fitted fringe position without reducing the fringe modulation. In contrast, spatial variations of the lattice intensity and differences in the atomic trajectories and lattice interaction can produce an inhomogeneous accumulated phase across the ensemble, which reduces the Ramsey-fringe modulation and may also distort the fitted fringe.

In the present experiment, the free-fall and lattice-assisted spectra were acquired in independent scans using the same microwave source, rather than in an interleaved differential measurement designed to isolate the lattice-induced contribution. Differences between the fitted fringe positions or phases of the two independent scans may therefore reflect a combination of the lattice-induced contribution and slow changes in the magnetic field, microwave-interaction conditions, and other experimental parameters. Consequently, the observed difference cannot be uniquely identified with ϕ_{lat}, and no absolute lattice-induced phase or frequency shift is extracted from the present data. The repeated lattice-assisted measurements in Fig. 3(c) show that the fitted initial phase is reproducible under the fixed lattice-assisted operating condition, but they do not provide an interleaved free-fall reference with which to isolate the lattice-induced phase. A quantitative determination of the lattice-induced shift would require, for example, interleaved measurements with and without the lattice under otherwise common experimental conditions.

This situation differs from that in conventional optical lattice clocks, where the trapping lattice is typically operated near a magic condition to suppress the differential AC Stark shift of the clock transition during long-duration trapping and interrogation [43–46]. In the present experiment, the 780-nm moving lattice instead acts as a transient momentum-transfer element during the Bloch-acceleration stage and is not operated at a magic condition. The present scheme is therefore optimized for active trajectory control rather than state-insensitive trapping. The relevant lattice-induced phase is accumulated only during the finite lattice-interaction stage and can in principle be reduced through optimization of the lattice depth, interaction sequence, and appropriate compensation techniques.

Second, the spatially nonuniform microwave field can affect both the run-to-run reproducibility and the equivalence of the two Ramsey interactions. As discussed in Sec. 3.2, redirecting the atoms toward the microwave-interaction region can make the conditions of the second microwave interaction more reproducible from one experimental realization to another, providing a plausible contribution to the smaller point-to-fit scatter in the lattice-assisted data. However, this does not imply that the first and second microwave interactions within a given Ramsey sequence are identical. Because the microwave radiation is delivered by a horn rather than a highly uniform cavity, the atomic position and velocity distributions at the second pulse can differ from those at the first pulse. The atoms can therefore sample different microwave amplitudes and phases at the two Ramsey interactions, producing differences in the effective pulse area, Ramsey phase, and fringe modulation.

For longer controlled trajectories, magnetic-field inhomogeneity can provide an additional source of phase variation. The use of the $m_F = 0$ clock states suppresses

the first-order Zeeman shift, but the second-order Zeeman shift remains sensitive to the magnetic-field magnitude. When the atoms sample a larger spatial region along the folded trajectory, magnetic-field gradients and bias-field fluctuations can therefore produce additional phase variations and reduce the Ramsey-fringe modulation.

4.3. Toward multiple-fold trajectory control

The single-fold demonstration presented here represents a first step toward multiple-fold trajectory control. In principle, repeated optical lattice momentum compensation could allow atoms to remain within a confined spatial region while accumulating a longer Ramsey evolution time. Such a multiple-fold configuration would distinguish the present active control approach from a simple ballistic fountain trajectory.

Realizing multiple-fold operation requires improvements in three directions. First, the microwave interaction region should be made more homogeneous, for example by using a stable microwave cavity, to reduce the mismatch between repeated Ramsey interactions. Second, the optical-lattice sequence should be optimized by minimizing the interaction time and improving the loading, sweep, and unloading waveforms to reduce differential light shifts and nonadiabatic losses. For microwave hyperfine transitions, engineered magic or near-magic trapping conditions provide one possible route to reducing differential lattice shifts [47, 48]. Related multi-frequency compensation approaches have also been considered and implemented in atom interferometry, where additional optical frequency components can be used to compensate AC Stark shifts [49]. Adapting such a compensation scheme to the present moving-lattice configuration may provide a possible route to reducing lattice-induced phase shifts while retaining efficient Bloch momentum transfer. Third, magnetic shielding, bias-field stabilization, and magnetic-gradient compensation should be improved to suppress phase changes induced by second-order Zeeman shifts. These improvements may allow multiple-fold Ramsey trajectories to support longer interrogation times in compact ultracold-atom systems.

5. Conclusion

We have demonstrated a single-fold trajectory folding scheme for microwave Ramsey interrogation of ultracold ^{87}Rb atoms by combining a moving optical lattice with momentum transfer based on Bloch oscillations. In this scheme, the moving lattice provides upward momentum compensation after the first microwave pulse and redirects the falling ultracold atoms back toward the microwave interaction region for the second pulse. The observed Ramsey fringes show that optical lattice trajectory control can be incorporated into microwave Ramsey coherent evolution while maintaining a reproducible Ramsey response.

In the present compact apparatus, the free-fall Ramsey configuration cannot provide a reliable fitted linewidth near the 5 Hz level, whereas the lattice-assisted configuration extends the interrogation time to $T = 151$ ms and yields a Ramsey linewidth of 3.12 ± 0.07 Hz, following the expected inverse-time narrowing trend. The quantitative fringe analysis further shows that extending the controlled Ramsey time is accompanied by a reduction in the fringe modulation depth, identifying coherence preservation as a key challenge for future multiple-fold trajectory control. Although the present work is limited to a single-fold demonstration, it establishes an experimental framework for replacing a purely ballistic Ramsey trajectory with an actively controlled one. Since the folding process is governed by electronically controlled optical lattice parameters, the Ramsey evolution time can be continuously adjusted without changing the mechanical structure of the apparatus. This tunability provides greater flexibility than a fixed ballistic fountain trajectory for parameter optimization and scenario-dependent adaptation in compact ultracold-atom systems. The approach therefore offers a technical route toward multiple-fold trajectory control and may be useful for atom-based precision measurements requiring long coherent evolution in limited spatial volumes.

Data availability statement

Data will be made available on request.

Acknowledgment

This work was supported by the National Key Research and Development Program of China (Grants No. 2021YFA0718300 and No. 2021YFA1400900) and the National Natural Science Foundation of China (Grant No. 92365208).

Conflict of interest

The authors declare no competing interests.

References

[1] Ramsey N F 1950 *Phys. Rev.* **78** 695

[2] Vanier J 2005 *Appl. Phys. B* **81** 421

[3] Wynands R and Weyers S 2005 *Metrologia* **42** S64

[4] Guéna J, Abgrall M, Rovera D, Laurent P, Chupin B, Lours M, Santarelli G, Rosenbusch P, Tobar M E, Li R, Gibble K, Clairon A and Bize S 2012 *IEEE Trans. Ultrason. Ferroelectr. Freq. Control* **59** 391

[5] Ludlow A D, Boyd M M, Ye J, Peik E and Schmidt P O 2015 *Rev. Mod. Phys.* **87** 637

[6] Ren W, Li T, Qu Q Z, Wang B, Li L, Lü D S, Chen W B and Liu L 2020 *Natl. Sci. Rev.* **7** 1828

[7] Liu L, Lü D S, Chen W B, et al. 2018 *Nat. Commun.* **9** 2760

[8] Deng S M D, Ren W, Xiang J F, Zhao J B, Li L, Zhang D, Wan J Y, Meng Y L, Jiang X J, Li T, Liu L and Lü D S 2024 *npj Microgravity* **10** 66

[9] Liu P, Meng Y L, Wan J Y, Wang X M, Wang Y N, Xiao L, Cheng H D and Liu L 2015 *Phys. Rev. A* **92** 062101

[10] Lee S, Choi G W, Hong H G, Kwon T Y, Lee S B, Heo M S and Park S E 2021 *Appl. Phys. Lett.* **119** 064002

[11] Bregazzi A, Batori E, Lewis B, Affolderbach C, Mileti G, Riis E and Griffin P F 2024 *Sci. Rep.* **14** 931

[12] Elvin R, Wright M W, Lewis B, Keliehor B L, Bregazzi A, McGilligan J P, Arnold A S, Griffin P F and Riis E 2020 *Adv. Opt. Technol.* **9** 297

[13] Ben Dahan M, Peik E, Reichel J, Castin Y and Salomon C 1996 *Phys. Rev. Lett.* **76** 4508

[14] Wilkinson S R, Bharucha C F, Madison K W, Niu Q and Raizen M G 1996 *Phys. Rev. Lett.* **76** 4512

[15] Peik E, Ben Dahan M, Bouchoule I, Castin Y and Salomon C 1997 *Phys. Rev. A* **55** 2989

[16] Anderson B P and Kasevich M A 1998 *Science* **282** 1686

[17] Morsch O and Oberthaler M 2006 *Rev. Mod. Phys.* **78** 179

[18] Cladé P, Guellati-Khélifa S, Nez F and Biraben F 2009 *Phys. Rev. Lett.* **102** 240402

[19] Müller H, Chiow S W, Long Q, Herrmann S and Chu S 2008 *Phys. Rev. Lett.* **100** 180405

[20] Chiow S W, Kovachy T, Chien H C and Kasevich M A 2011 *Phys. Rev. Lett.* **107** 130403

[21] McDonald G D, Kuhn C C N, Bennetts S, Debs J E, Hardman K S, Johnsson M, Close J D and Robins N P 2013 *Phys. Rev. A* **88** 053620

[22] Kovachy T, Asenbaum P, Overstreet C, Donnelly C A, Dickerson S M, Sugarbaker A, Hogan J M and Kasevich M A 2015 *Nature* **528** 530

[23] Gebbe M, Siemß J N, Gersemann M, Müntinga H, Herrmann S, Lämmerzahl C, Ahlers H, Gaaloul N, Schubert C, Hammerer K, Abend S and Rasel E M 2021 *Nat. Commun.* **12** 2544

[24] Fitzek F, Kirsten-Siemß J N, Rasel E M, Gaaloul N and Hammerer K 2024 *Phys. Rev. Res.* **6** L032028

[25] Narducci F A, Black A T and Burke J H 2022 *Adv. Phys. X* **7** 1946426

[26] Kasevich M and Chu S 1991 *Phys. Rev. Lett.* **67** 181

[27] Peters A, Chung K Y and Chu S 1999 *Nature* **400** 849

[28] Cronin A D, Schmiedmayer J and Pritchard D E 2009 *Rev. Mod. Phys.* **81** 1051

[29] Young B, Kasevich M and Chu S 1997 Precision atom interferometry with light pulses in *Atom Interferometry* ed P R Berman (San Diego: Academic Press) pp. 363–406

[30] Peng P, Mao D, Liang Y, Yin G, Shui H, Song B and Zhou X 2025 *Phys. Rev. A* **112** 053313

[31] Yin G, Lai C K, Chang N, Liang Y, Mao D and Zhou X 2024 *Front. Phys.* **19** 62201

[32] Yin G, Kong L, Yu Z, Tian J, Chen X and Zhou X 2023 *Phys. Rev. A* **108** 033310

[33] Yu Z, Tian J, Peng P, Mao D, Chen X and Zhou X 2023 *Phys. Rev. A* **107** 023303

[34] Hu D, Niu L, Jin S, Chen X, Dong G, Schmiedmayer J and Zhou X 2018 *Commun. Phys.* **1** 29

[35] Zhou X, Jin S and Schmiedmayer J 2018 *New J. Phys.* **20** 055005

[36] Dong X, Wu C, Yu Z, Tian J, Wang Z, Chen X, Jin S and Zhou X 2022 *Opt. Express* **30** 41437

[37] Hu D, Jin S, Yu Z, Shui H, Wang Y and Zhou X 2023 *Opt. Express* **31** 41149

[38] Anderson M H, Ensher J R, Matthews M R, Wieman C E and Cornell E A 1995 *Science* **269** 198

[39] Davis K B, Mewes M O, Andrews M R, van Druten N J, Durfee D S, Kurn D M and Ketterle W 1995 *Phys. Rev. Lett.* **75** 3969

[40] Ketterle W, Durfee D S and Stamper-Kurn D M 1999 Making, probing and understanding Bose-Einstein condensates in *Bose-Einstein Condensation in Atomic Gases* ed M Inguscio, S Stringari and C E Wieman (Amsterdam: IOS Press) pp. 67–176

[41] Grimm R, Weidemüller M and Ovchinnikov Y B 2000 *Adv. At. Mol. Opt. Phys.* **42** 95

[42] Steck D A 2025 *Rubidium 87 D Line Data*, available online at `http://steck.us/alkalidata` (revision 2.3.4, 8 August 2025)

[43] Katori H, Takamoto M, Pal'chikov V G and Ovsiannikov V D 2003 *Phys. Rev. Lett.* **91** 173005

[44] Takamoto M, Hong F L, Higashi R and Katori H 2005 *Nature* **435** 321

[45] Ye J, Kimble H J and Katori H 2008 *Science* **320** 1734

[46] Derevianko A and Katori H 2011 *Rev. Mod. Phys.* **83** 331

[47] Beloy K, Derevianko A, Dzuba V A and Flambaum V V 2009 *Phys. Rev. Lett.* **102** 120801

[48] Lundblad N, Schlosser M and Porto J V 2010 *Phys. Rev. A* **81** 031611

[49] Kim M, Notermans R, Overstreet C, Curti J, Asenbaum P and Kasevich M A 2020 *Opt. Lett.* **45** 6555